Springer

KSME

Journal of Mechanical Science and Technology 28 (7) (2014) 2749~2757

www.springerlink.com/content/1738-494x
DOI 10.1007/s12206-014-0514-7

Research on gear shaping strategy for internal helical non-circular gears and performance analyses for linkage models †

Youyu Liu*

School of Mechanical and Automotive Engineering, Anhui Polytechnic University, Wuhu, 241000, China

(Manuscript Received March 19, 2013; Revised January 9, 2014; Accepted February 19, 2014)

Abstract

Gear shaping is an efficient cutting method available for internal helical non-circular gears, but gear hobbing is not. Four methods and models of generating motion were built. Virtual shaping revealed that the method of equal arc-length of gear billet has the highest machining precision. Three methods of primary motion were built and analyzed respectively by using a kinetic simulation, which revealed that the method of keeping a constant velocity has the best dynamic performance. Two methods of additional motion were offered. Virtual shaping revealed that the two methods have the same precision, whether the gear has a right-hand helix or left-hand helix. Finally, two optimal shaping models were provided, and performed shaping experiments, respectively. The experiments showed that the shaping strategies and models are correct and feasible. Tooth-flank detections revealed that every tooth of the gears has the same precision using the optimal shaping models.

Keywords: Helical non-circular gears; Internal gears; Gear shaping; Linkage models; Tooth accuracy

1. Introduction

Non-circular gears combine the advantages of both cylindrical gears and cams, not only can be used for accurate transmission with a continuously variable ratio [1], but also can actualize accurate non-circular movement [2]. Non-circular gears are some kinds of irreplaceable parts in the field of agricultural machineries, vehicles, or fluid machineries [3-5], for they can deliver a high output power. Although having been around at least since 1930s, the studies of non-circular gears develop slowly, for their wide range, various complex shape, cumbersome calculation or design, in particular difficult manufacturing process. In recent years, with the development of computerized numerical control (CNC, non-circular gears have become a hot spot because of re-invention [1-6]. With the rapid developing of wire-electrode cutting, spur non-circular gears have been used broadly [7]. However, wire-electrode cutting is inefficient, and difficult to cut helical non-circular gears. Cylindrical helical gears have the advantages of steady transmission, small vibration, and low noise during meshing process [8]. Helical non-circular gears have the same advantages, and can be used in the occasions with high-speed, heavy-load, or low-noise.

Up to now, because of lacking efficient manufacturing technology, helical non-circular gears have rarely applied to industrial production and daily life. In addition to wire-electrode cutting, there are some other new manufacturing methods such as electrical discharge machining (EDM) [9] and laser machining [10] for non-circular gear. However, those methods are extremely inefficient and not suitable for manufacturing helical non-circular gears. In addition, they are suitable only for manufacturing such as ones with special materials or extreme thinness. Precision forging technology [11], as a highly efficient process, can be used for manufacturing helical non-circular gears. However, there is no accumulation in the mold machining technology used for helical non-circular gears, and in the measuring technique of molds or gears. Moreover, 3-D printing or rapid prototyping [12] can be also used for manufacturing helical non-circular gears in theory. Nevertheless, gears with section piled cannot meet the mechanical properties required during the transmission process. Because they are efficient and can adopt forging piece as a gear billet, both gear hobbing and gear shaping are two preferred choices for manufacturing helical non-circular gears [13].

We had constructed some available hobbing schemes using gear hobbing for helical non-circular gears based on a four-axis linkage [14] and a five-axis linkage [15] respectively, and had singled out two excellent strategies with their linkage models progressively. Moreover, we had built another hobbing scheme for it based on the method of axial shift of hob in

*Corresponding author. Tel.: +82 13965184758, Fax.: +82 5532871252
E-mail address: liuyyu@ahpu.edu.cn
† Recommended by Associate Editor Ki-Hoon Shin

article [16], which can expand the operating range of a machine tool and improve a tool life by comparing to the strategies of meshing point on hob fixed [14, 15].

Helical non-circular gears can be classified into two main categories, internal ones and external ones. Internal helical non-circular gears can be applied to planetary mechanism with a continuously variable ratio. The dominant feature of those gears is that tip surfaces are located within their pitch curves. Thus, cutters should be located within the pitch curves in cutting processing. As for gear hobbing, based on the generating principle of helical tooling rack [14-16], the middle line of a rack is a straight line, which leads to the middle line pass through the pitch curve of gears, and then over cutting will occur. So gear hobbing is not fit for internal gears. The principle of gear shaping is based on the meshing theory of non-circular gear [17], which reveals that internal helical non-circular gears can be shaped while the pitch radius of shaper cutter is less than the minimum curvature of the pitch curve of gears.

In this study, based on the motion features of internal gear shaping, several linkage models are built which include a generating motion between shaper cutter and gear billet, a primary motion of shaper cutter, and an additional motion of shaper cutter or gear billet. Shaping accuracy or dynamic performance of each model has been analyzed by using virtual machining or dynamics analysis. Thus, two optimal shaping models have been built progressively. Both of optimal shaping models and virtual machining have been demonstrated to be valid by using gear shaping experiments and tooth-flank detections.

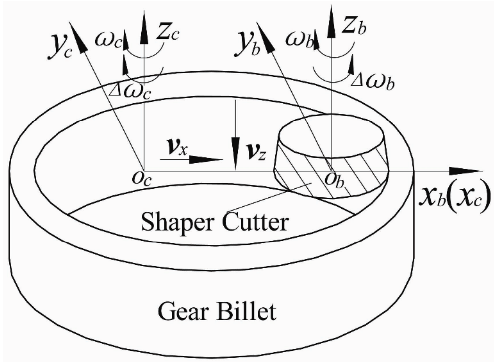

Fig. 1. Schematic diagram of gear shaping.

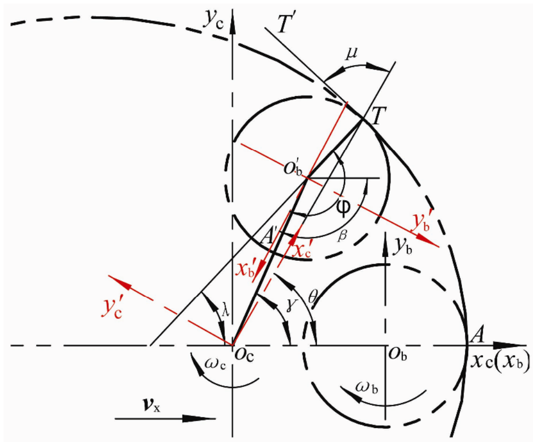

Fig. 2. Section of gear billet on end-face.

2. Gear shaping strategy for internal helical non-circular gears

As shown in Fig. 1, the pitch circle of shaper cutter, revolving as ω_b, and the pitch curve of gear billet, revolving as ω_c, are in continuous pure rolling contract in the same direction. The ω_b keeps a strict ratio with the ω_c, which generates a generating motion [17]. To keep the pitch circle internal tangent with the pitch curve, the gear billet must move along the *x*-axis (v_x). In addition, the shaper cutter should move downward along the *z*-axis (v_z), namely primary motion. There is an additional motion of shaper cutter ($\Delta\omega_b$), or that of gear billet ($\Delta\omega_c$), to generate the helixes of helical non-circular gears. Hence, it is a CNC gear shaper with four-axis linkage.

As shown in Fig. 2, $S_b(o_b\text{-}x_b y_b z_b)$ is a cutting tool coordinate system, the origin o_b of which is located at the center point of the lower end-surface of shaper cutter, and the axis z_b of which is coincident with the spindle of shaper cutter. The $S_b(o_b\text{-}x_b y_b z_b)$ revolves synchronously with the shaper cutter. $S_c(o_c\text{-}x_c y_c z_c)$, fixed in space, is a gear billet coordinate system, the origin o_c of which is located at the rotation-center of gear billet, and the axis z_c of which is coincident with the spindle of gear billet. x_c-axis passes through the point o_b, and is coincident with x_b-axis. Each axis of the $S_c(o_c\text{-}x_c y_c z_c)$ is independently parallel to that of the $S_b(o_b\text{-}x_b y_b z_b)$. A polar coordinate system that has a pole (o_c) and a polar axis (x_c) is built. The pitch curve equation of the gears is $r = r(\theta)$. The modulus of the polar radius is r, and the polar angle is θ. The point A is a starting point while shaping.

3. Generating motion between shaper cutter and gear billet

3.1 Linkage models

The generating motion between shaper cutter and gear billet in plane should follow the meshing theory of non-circular gear [17]. As shown in Fig. 2, in order to display shaping process in plane, the generating motion can be analyzed by taking a section of gear billet on end-face as the stationary frame of reference. The shaper cutter rotates in a clockwise direction, and orbits around the gear billet in a counterclockwise direction. After a while, the cutter location moves from point o_b to point o_b', and then the $S_b(o_b\text{-}x_b y_b z_b)$ turns into the $S_b'(o_b'\text{-}x_b' y_b' z_b')$. The shaper cutter orbits a degree of λ, and rotates an angle ϕ on its axis. The rotation angle of that relative to the gear billet is β. The TT' is a common tangent between the pitch circle of shaper cutter and the pitch curve of gear billet in the point T. The angle between the polar radius and the common tangent is μ [17].

$$\mu = \arctan\left[r/\left(\mathrm{d}r/\mathrm{d}\theta\right)\right] \qquad (0 \le \mu < \pi) \tag{1}$$

From Eq. (1),

$$\begin{cases} \sin\mu = r\Big/\sqrt{r^2 + \left(\mathrm{d}r/\mathrm{d}\theta\right)^2} \\ \cos\mu = \left(\mathrm{d}r/\mathrm{d}\theta\right)\Big/\sqrt{r^2 + \left(\mathrm{d}r/\mathrm{d}\theta\right)^2} \\ \dfrac{\mathrm{d}\mu}{\mathrm{d}\theta} = \dfrac{\left(\mathrm{d}r/\mathrm{d}\theta\right)^2 - r\left(\mathrm{d}^2r/\mathrm{d}\theta^2\right)}{r^2 + \left(\mathrm{d}r/\mathrm{d}\theta\right)^2} \end{cases}. \tag{2}$$

According to the principle of trigonometric function [18], we can infer the following in $\Delta T o_{\mathrm{b}}' o_{\mathrm{c}}$.

$$l = \left|o_{\mathrm{b}}' o_{\mathrm{c}}\right| = \sqrt{r^2 + r_{\mathrm{p}}^2 \text{-} 2 r r_{\mathrm{p}} \sin\mu} \tag{3}$$

$$l\sin\left(\gamma \text{-} \theta\right) = r_{\mathrm{p}}\cos\mu \tag{4}$$

where the r_{p} is the pitch radius of shaper cutter.

From Eq. (3),

$$\frac{\mathrm{d}l}{\mathrm{d}\theta} = \frac{r\,\mathrm{d}r/\mathrm{d}\theta \text{-} r_{\mathrm{p}}\sin\mu\,\mathrm{d}r/\mathrm{d}\theta \text{-} r r_{\mathrm{p}}\cos\mu\,\mathrm{d}\mu/\mathrm{d}\theta}{l}. \tag{5}$$

Consequently,

$$v_{\mathrm{x}} = \frac{\mathrm{d}l}{\mathrm{d}t} = \frac{r\,\mathrm{d}r/\mathrm{d}\theta \text{-} r_{\mathrm{p}}\sin\mu\,\mathrm{d}r/\mathrm{d}\theta \text{-} r r_{\mathrm{p}}\cos\mu\,\mathrm{d}\mu/\mathrm{d}\theta}{l}\omega \tag{6}$$

where the ω, equals to $\mathrm{d}\theta/\mathrm{d}t$, is the polar-angular velocity of gear billet.

While the cutter location moves from point o_{b} to point o_{b}' and the pitch circle of shaper cutter is pure rolling along the pitch curve of gear billet from point *A* to point *T*, the meshing arc length $A'T$ on the pitch circle of shaper cutter is equal to the arc length AT on the pitch curve of gear billet. That is to say,

$$s = \int_0^{\theta}\sqrt{r^2 + \left(\mathrm{d}r/\mathrm{d}\theta\right)^2}\,\mathrm{d}\theta \tag{7}$$

$$\phi = \lambda + \beta = s/r_{\mathrm{p}}. \tag{8}$$

The angular velocity ω_{b} of shaper cutter is as follows.

$$\omega_{\mathrm{b}} = \frac{\mathrm{d}\phi}{\mathrm{d}t} = \frac{\sqrt{r^2 + \left(\mathrm{d}r/\mathrm{d}\theta\right)^2}}{r_{\mathrm{p}}}\omega. \tag{9}$$

As shown in Fig. 2, $\lambda = \mu + \theta \text{-} \pi/2$. From Eq. (8),

$$\beta = s/r_{\mathrm{p}} \text{-} \mu \text{-} \theta + \pi/2. \tag{10}$$

Taking the derivative of Eq. (10) and simplifying it,

$$\omega_{\mathrm{r}} = \omega_{\mathrm{b}} \text{-} \frac{2\left(\mathrm{d}r/\mathrm{d}\theta\right)^2 - r\left(\mathrm{d}^2r/\mathrm{d}\theta^2\right) + r^2}{r^2 + \left(\mathrm{d}r/\mathrm{d}\theta\right)^2}\omega \tag{11}$$

where the angular velocity ω_{r} of shaper cutter relative to gear billet is $\mathrm{d}\beta/\mathrm{d}t$.

From Eq. (4),

$$\gamma = \theta + \arcsin\left(r_{\mathrm{p}}\cos\mu/l\right). \tag{12}$$

Taking the derivative of Eq. (12) and simplifying it,

$$\omega_{\mathrm{c}} = \omega - r_{\mathrm{p}}\frac{l\sin\mu\,\mathrm{d}\mu/\mathrm{d}\theta + \cos\mu\,\mathrm{d}l/\mathrm{d}\theta}{l^2\sqrt{1\text{-}\left(r_{\mathrm{p}}\cos\mu/l\right)^2}}\omega \tag{13}$$

where the angular velocity ω_{c} of gear billet is $\mathrm{d}\gamma/\mathrm{d}t$.

A basic linkage model of generating motion in plane can be established from Eqs. (6), (9), (11) and (13). There are four methods for non-circular gear shaping in plane: (1) equal rotary-angle of shaper cutter relative to gear billet (ERASCRGB; (2) equal arc-length of gear billet (EALGB; (3) equal rotary-angle of gear billet (ERAGB; (4) equal polar-angle of gear billet (EPAGB.

ERASCRGB implies that the revolving velocity (ω_{r}) of shaper cutter keeps constant. Based on a fundamental frequency ω_{r}, the basic linkage model can be transformed into a linkage model of ERASCRGB (see Eq. (14)).

$$\begin{aligned} v_{\mathrm{x}} &= \frac{\left[r\dfrac{\mathrm{d}r}{\mathrm{d}\theta} \text{-} r_{\mathrm{p}}\sin\mu\dfrac{\mathrm{d}r}{\mathrm{d}\theta} \text{-} r r_{\mathrm{p}}\cos\mu\dfrac{\mathrm{d}\mu}{\mathrm{d}\theta}\right]\left[r_{\mathrm{p}}r^2 + r_{\mathrm{p}}\left(\dfrac{\mathrm{d}r}{\mathrm{d}\theta}\right)^2\right]}{l\left[r^2 + \left(\dfrac{\mathrm{d}r}{\mathrm{d}\theta}\right)^2\right]^{\frac{3}{2}} - 2lr_{\mathrm{p}}\left(\dfrac{\mathrm{d}r}{\mathrm{d}\theta}\right)^2 + lrr_{\mathrm{p}}\dfrac{\mathrm{d}^2r}{\mathrm{d}\theta^2} - lr_{\mathrm{p}}r^2}\omega_{\mathrm{r}} \\ \omega_{\mathrm{c}} &= \frac{\left[l^2\sqrt{1\text{-}\left(\dfrac{r_{\mathrm{p}}\cos\mu}{l}\right)^2} - lr_{\mathrm{p}}\sin\mu\dfrac{\mathrm{d}\mu}{\mathrm{d}\theta} - r_{\mathrm{p}}\cos\mu\dfrac{\mathrm{d}l}{\mathrm{d}\theta}\right]\left[r_{\mathrm{p}}r^2 + r_{\mathrm{p}}\left(\dfrac{\mathrm{d}r}{\mathrm{d}\theta}\right)^2\right]}{l^2\sqrt{1\text{-}\left(\dfrac{r_{\mathrm{p}}\cos\mu}{l}\right)^2}\left[\left[r^2 + \left(\dfrac{\mathrm{d}r}{\mathrm{d}\theta}\right)^2\right]^{\frac{3}{2}} - 2r_{\mathrm{p}}\left(\dfrac{\mathrm{d}r}{\mathrm{d}\theta}\right)^2 + rr_{\mathrm{p}}\dfrac{\mathrm{d}^2r}{\mathrm{d}\theta^2} - r_{\mathrm{p}}r^2\right]}\omega_{\mathrm{r}} \\ \omega_{\mathrm{b}} &= \frac{\left[r^2 + \left(\dfrac{\mathrm{d}r}{\mathrm{d}\theta}\right)^2\right]^{\frac{3}{2}}}{\left[r^2 + \left(\dfrac{\mathrm{d}r}{\mathrm{d}\theta}\right)^2\right]^{\frac{3}{2}} - 2r_{\mathrm{p}}\left(\dfrac{\mathrm{d}r}{\mathrm{d}\theta}\right)^2 + rr_{\mathrm{p}}\dfrac{\mathrm{d}^2r}{\mathrm{d}\theta^2} - r_{\mathrm{p}}r^2}\omega_{\mathrm{r}} \end{aligned}. \tag{14}$$

EALGB implies that gear billet rotates the same arc-length in the same time, and then the revolving velocity (ω_{b}) of cutting tool coordinate system keeps constant. Based on a fundamental frequency ω_{b}, the basic linkage model can be trans-

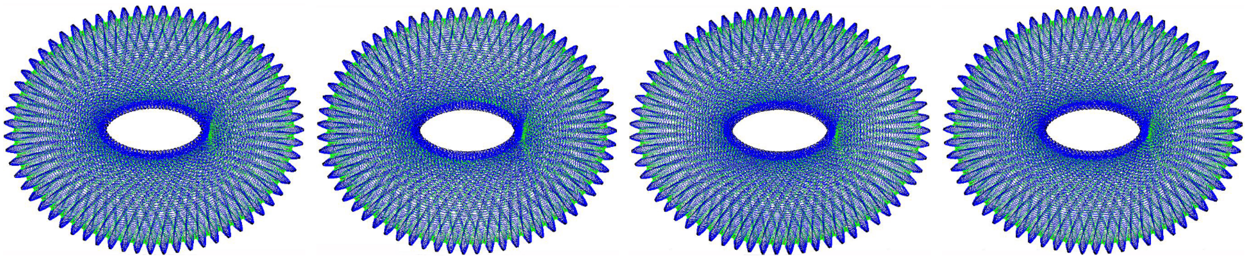

(a) ERASCRGB (b) EALGB (c) ERAGB (d) EPAGB

Fig. 3. Virtual shaping of generating motion.

formed into a linkage model of EALGB (see Eq. (15)).

$$
\begin{aligned}
v_x &= \frac{r r_p \dfrac{dr}{d\theta} - r_p^2 \sin\mu \dfrac{dr}{d\theta} - r r_p^2 \cos\mu \dfrac{d\mu}{d\theta}}{l\sqrt{r^2 + \left(\dfrac{dr}{d\theta}\right)^2}}\omega_b \\
\omega_c &= \frac{l^2\sqrt{1-\left(\dfrac{r_p\cos\mu}{l}\right)^2} r_p - l r_p^2 \sin\mu \dfrac{d\mu}{d\theta} - r_p^2\cos\mu\dfrac{dl}{d\theta}}{l^2\sqrt{1-\left(\dfrac{r_p\cos\mu}{l}\right)^2}\sqrt{r^2+\left(\dfrac{dr}{d\theta}\right)^2}}\omega_b
\end{aligned} . \quad (15)
$$

ERAGB implies that the revolving velocity (ω_c) of gear billet keeps constant. Based on a fundamental frequency ω_c, the basic linkage model can be transformed into a linkage model of ERAGB (see Eq. (16)).

$$
\begin{aligned}
v_x &= \frac{l\sqrt{1-\left(\dfrac{r_p\cos\mu}{l}\right)^2}\left[r\dfrac{dr}{d\theta} - r_p\sin\mu\dfrac{dr}{d\theta} - r r_p\cos\mu\dfrac{d\mu}{d\theta}\right]\omega_c}{l^2\sqrt{1-\left(\dfrac{r_p\cos\mu}{l}\right)^2} - l r_p \sin\mu\dfrac{d\mu}{d\theta} - r_p\cos\mu\dfrac{dl}{d\theta}} . \\
\omega_b &= \frac{l^2\sqrt{r^2+\left(\dfrac{dr}{d\theta}\right)^2}\sqrt{1-\left(\dfrac{r_p\cos\mu}{l}\right)^2}\,\omega_c}{l^2 r_p\sqrt{1-\left(\dfrac{r_p\cos\mu}{l}\right)^2} - l r_p^2\sin\mu\dfrac{d\mu}{d\theta} - r_p^2\cos\mu\dfrac{dl}{d\theta}}
\end{aligned} \quad (16)
$$

EPAGB implies that the revolving velocity (ω) of gear billet keeps constant. Based on a fundamental frequency ω, the basic linkage model can be transformed into a linkage model of EPAGB (see Eq. (17)).

$$
\begin{aligned}
v_x &= \frac{r\dfrac{dr}{d\theta} - r_p\sin\mu\dfrac{dr}{d\theta} - r r_p\cos\mu\dfrac{d\mu}{d\theta}}{l}\omega \\
\omega_b &= \frac{\sqrt{r^2+\left(\dfrac{dr}{d\theta}\right)^2}}{r_p}\omega \\
\omega_c &= \frac{l^2\sqrt{1-\left(\dfrac{r_p\cos\mu}{l}\right)^2} - l r_p\sin\mu\dfrac{d\mu}{d\theta} - r_p\cos\mu\dfrac{dl}{d\theta}}{l^2\sqrt{1-\left(\dfrac{r_p\cos\mu}{l}\right)^2}}\omega .
\end{aligned} \quad (17)
$$

3.2 Virtual shaping of generating motion

In order to analyze and compare the features of the four methods for non-circular gear shaping, an internal helical oval gear [19], as a typical helical non-circular gear, is shaped virtually by Matlab respectively according to the four linkage models Eqs. (14)-(17). The parameters of the internal helical oval gear are as follows: major semi-axis (a) is 120 mm; tooth width (b) is 50 mm; eccentricity (e) is 0.1; order (n) of ellipse is 2; normal module (m_n) is 3.75 mm; helix angle (β_c) is 11.617°; tooth number (Z) of gear is 63; tooth number (z) of shaper cutter is 22. The shaping parameters are as follows: processing time (t) of shaping one cycle along pitch curve is 1260 seconds; single-cycle period τ is 0.5 s; shaping time t' in a single-cycle period is 0.2 s. The virtual shaping results are shown in Fig. 3, which shows that the four methods for non-circular gear shaping are all feasible, but the distributions of cutting marks among every tooth of various methods are obviously different.

When a stroke happens, a cutting mark is generated on teeth-profile surface. Distributions of cutting marks among every tooth of various methods are shown in Fig. 4, number of gear teeth runs from 1 to 63 while θ runs from 0 to 2π. The cutting marks among every tooth by ERAGB are the most uneven. For instance, there are 29 cutting marks on the 1st tooth and the 32nd tooth, respectively, and 55 cutting marks on the 16th tooth and the 48th tooth, respectively. The cutting marks among every tooth by ERASCRGB, being uneven second to the method of ERAGB, range from 33 to 46. The cutting marks among every tooth by EPAGB range from 36 to 45, and are more uniform than the first two. The cutting marks among every tooth by EALGB are 40, which are uniform and consistent. The more cutting marks on a gear tooth, the more accurate the tooth-profile surface enveloped by shaper cutter would be. Furthermore, the precision of a helical non-circular gear should be measured at its lowest level. Consequently, a

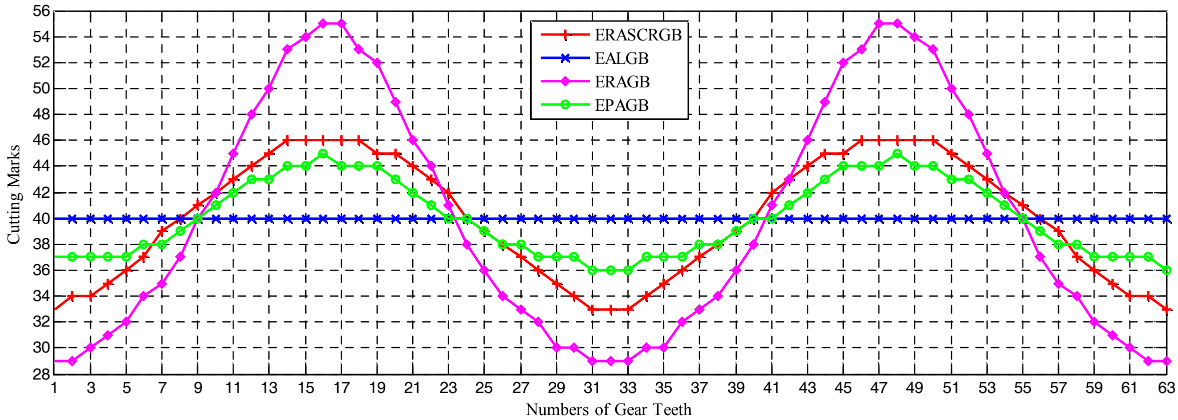

Fig. 4. Distribution of cutting marks among every tooth.

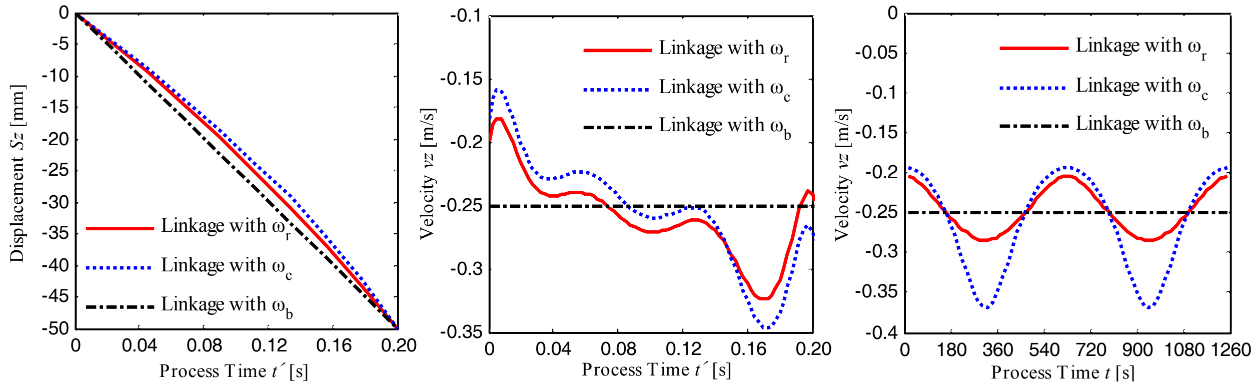

(a) Shaping displacement on the 1st tooth (b) Shaping velocity on the 1st tooth (c) Shaping velocity along the pitch curve ($S_z = 0$)

Fig. 5. Features of primary motion.

gear shaped by EALGB has the highest accuracy under a given efficiency, closely followed by EPAGB and ERASCRGB, and then ERAGB. The method of EALGB should be adopted for the generating motion in plane.

4. Primary motion

4.1 Linkage models

The primary motion (v_z) can be linked with ω_b (see Eq. (18)), and can be linked with ω_c (see Eq. (19)), also can be linked with ω_r (see Eq. (20)). As for Eq. (18) to the method of EALGB, v_z will keep a constant velocity independently because of ω_b is constant.

$$v_z = k_1\omega_b \tag{18}$$

$$v_z = k_2\omega_c \tag{19}$$

$$v_z = k_3\omega_r \tag{20}$$

where the k_1, the k_2, and the k_3 are constant coefficients.

4.2 Kinematic analysis of primary motion

As shown in Fig. 5(a), there is several different in the curves (S_z) of shaping displacement on the 1st tooth for the three linkage models. The displacement curve of linkage with ω_t is a line with a constant slope. However, the slope of other two displacement curves is continuously changing. As shown in Fig. 5(b), there is obviously different in the curves (v_z) of shaping velocity on the 1st tooth for the three linkage models. The velocity curve of linkage with ω_t is a line with a constant value, and then the shaping force of that keeps stable for its acceleration is zero. However, the fluctuating range of other two velocity curves is higher, and then the control of the system becomes rather difficult for their bad dynamic performances. The curves (v_z) of shaping velocity along the pitch curve are shown in Fig. 5(c) while S_z is zero. The velocity curve of linkage with ω_t is a line with an unchanging value, which implies that its acceleration is identically equal to zero. Nevertheless, the range of other two velocity curves fluctuates sharply, which makes the system control difficult. Consequently, the method of linkage with ω_t is appropriate to adopt for its stable shaping force and its good dynamic performances.

5. Additional motion

5.1 Linkage models

For helical gears, there are two methods to conduct addi-

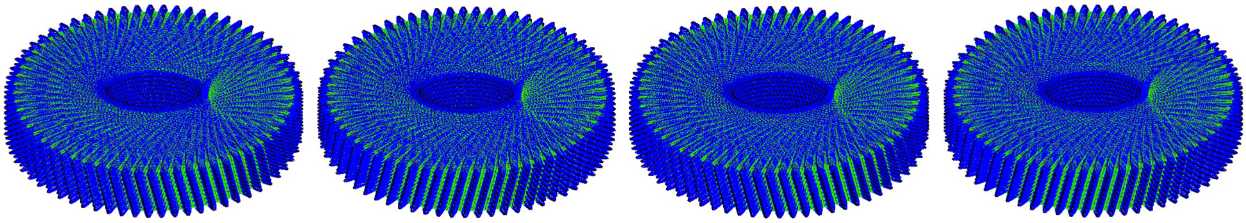

(a) Additional motion of shaper cutter & left-hand helix (b) Additional motion of shaper cutter & right-hand helix (c) Additional motion of gear billet & left-hand helix (d) Additional motion of gear billet & right-hand helix

Fig. 6. Virtual shaping of additional motion.

tional motion in a shaping stroke. One is additional motion of shaper cutter, and another is additional motion of gear billet. The additional motion of shaper cutter implies that shaper cutter should rotate a week additionally while moving downward or upward a screw lead of shaper cutter along principal shaft [20]. Hence, the additional motion of shaper cutter ($\Delta\omega_{\mathrm{b}}$) is as follows.

$$\Delta\omega_{\mathrm{b}} = v_{\mathrm{z}} \tan\beta_{\mathrm{c}} / r_{\mathrm{p}} \tag{21}$$

where the β_{c} is the helix angle of helical gear.

The resultant angular-velocity (ω_{b}^{*}) of shaper cutter is as follows.

$$\omega_{\mathrm{b}}^{*} = \omega_{\mathrm{b}} \pm \Delta\omega_{\mathrm{b}} \tag{22}$$

where "-" is adopted while shaper cutter rotates in the same direction as the helical sense of its teeth; otherwise, "+" is adopted.

The additional motion of gear billet implies that gear billet should rotate a week additionally while shaper cutter moves downward or upward a screw lead of gear billet along principal shaft [20]. So the additional motion of gear billet ($\Delta\omega_{\mathrm{c}}$) is as follows.

$$\int_0^{t'} r\Delta\omega_{\mathrm{c}} dt' = \int_0^{t'} \tan\beta_{\mathrm{c}} v_{\mathrm{z}} dt' \,. \tag{23}$$

Taking the derivative of Eq. (23) and simplifying it,

$$\Delta\omega_{\mathrm{c}} = v_{\mathrm{z}} \tan\beta_{\mathrm{c}} / r \,. \tag{24}$$

The resultant angular-velocity (ω_{c}^{*}) of gear billet is as follows.

$$\omega_{\mathrm{c}}^{*} = \omega_{\mathrm{c}} \pm \Delta\omega_{\mathrm{c}} \tag{25}$$

where "+" is adopted while shaper cutter rotates in the same direction as the helical sense of its teeth; otherwise, "-" is adopted.

5.2 Virtual shaping of additional motion

As shown in Fig. 6, based on EALGB and the method of linkage with ω_{t} , some left-hand helical gears and right-hand ones are shaped virtually by additional motion of shaper cutter or that of gear billet respectively. Shaping results reveal that the two methods of additional motion are all correct and feasible, and the different additional motion has no effect on the shaping accuracy of left-hand helical gears or right-hand ones. Therefore, the two methods of additional motion are acceptable.

6. Optimal shaping models

In conclusion, a shaping model adopting EALGB in plane and the method of linkage with ω_{b} in vertical direction is the best strategy. Moreover, from Eqs. (15), (20)-(22), an optimal shaping model adopting the method of additional motion of shaper cutter is as Eq. (26).

From Eqs. (15), (20), (24), (25), another optimal shaping model adopting the method of additional motion of gear billet is as Eq. (27).

$$\begin{aligned} v_{\mathrm{x}} &= \frac{r r_{\mathrm{p}} \dfrac{\mathrm{d}r}{\mathrm{d}\theta} - r_{\mathrm{p}}^2 \sin\mu \dfrac{\mathrm{d}r}{\mathrm{d}\theta} - r r_{\mathrm{p}}^2 \cos\mu \dfrac{\mathrm{d}\mu}{\mathrm{d}\theta}}{l\sqrt{r^2 + \left(\dfrac{\mathrm{d}r}{\mathrm{d}\theta}\right)^2}} \omega_{\mathrm{b}} \\ v_{\mathrm{z}} &= k_1 \omega_{\mathrm{b}} \\ \omega_{\mathrm{c}} &= \frac{l^2 \sqrt{1 - \left(\dfrac{r_{\mathrm{p}} \cos\mu}{l}\right)^2} r_{\mathrm{p}} - l r_{\mathrm{p}}^2 \sin\mu \dfrac{\mathrm{d}\mu}{\mathrm{d}\theta} - r_{\mathrm{p}}^2 \cos\mu \dfrac{\mathrm{d}l}{\mathrm{d}\theta}}{l^2 \sqrt{1 - \left(\dfrac{r_{\mathrm{p}} \cos\mu}{l}\right)^2} \sqrt{r^2 + \left(\dfrac{\mathrm{d}r}{\mathrm{d}\theta}\right)^2}} \omega_{\mathrm{b}} \\ \omega_{\mathrm{b}}^{*} &= \omega_{\mathrm{b}} \pm \frac{v_{\mathrm{z}} \tan\beta_{\mathrm{c}}}{r_{\mathrm{p}}} \end{aligned} \tag{26}$$

$$\begin{aligned} v_{\mathrm{x}} &= \frac{r r_{\mathrm{p}} \dfrac{\mathrm{d}r}{\mathrm{d}\theta} - r_{\mathrm{p}}^2 \sin\mu \dfrac{\mathrm{d}r}{\mathrm{d}\theta} - r r_{\mathrm{p}}^2 \cos\mu \dfrac{\mathrm{d}\mu}{\mathrm{d}\theta}}{l\sqrt{r^2 + \left(\dfrac{\mathrm{d}r}{\mathrm{d}\theta}\right)^2}} \omega_{\mathrm{b}} \\ v_{\mathrm{z}} &= k_1 \omega_{\mathrm{b}} \\ \omega_{\mathrm{c}}^{*} &= \frac{l^2 \sqrt{1 - \left(\dfrac{r_{\mathrm{p}} \cos\mu}{l}\right)^2} r_{\mathrm{p}} - l r_{\mathrm{p}}^2 \sin\mu \dfrac{\mathrm{d}\mu}{\mathrm{d}\theta} - r_{\mathrm{p}}^2 \cos\mu \dfrac{\mathrm{d}l}{\mathrm{d}\theta}}{l^2 \sqrt{1 - \left(\dfrac{r_{\mathrm{p}} \cos\mu}{l}\right)^2} \sqrt{r^2 + \left(\dfrac{\mathrm{d}r}{\mathrm{d}\theta}\right)^2}} \omega_{\mathrm{b}} \pm \frac{v_{\mathrm{z}} \tan\beta_{\mathrm{c}}}{r} \end{aligned} \tag{27}$$

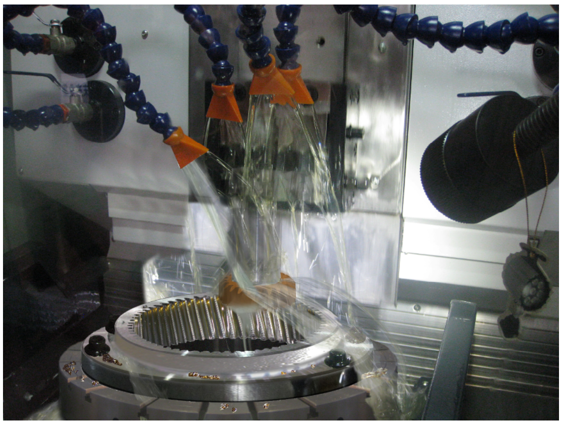

Fig. 7. Shaping process of internal helical oval gears.

(a) Internal right-hand oval gear (b) Internal left-hand oval gear

Fig. 8. Shaping outcomes of internal helical oval gears.

7. Shaping experiments and tooth-flank detections

Based on the two optimal shaping models Eqs. (26) and (27), two shaping modules for helical non-circular gears have been developed on a shaping platform with ARM (advanced RISC machines) & DSP (digital signal processor) & FPGA (field programmable gata array) [21]. Two internal helical oval gears (one is right-hand and the other is left-hand, their other parameters are as mentioned are shaped factually with the two shaping modules, as shown in Fig. 7. The shaping outcomes of internal helical oval gears are shown in Fig. 8. The internal right-hand oval gear shown in Fig. 8(a) is shaped with the model Eq. (26). Moreover, the right-hand one in Fig. 8(b) is shaped with the model Eq. (27). The shaping experiments show that the optimal shaping schemes and their linkage models are correct and feasible.

An additional motion will lead to the acceleration of shaper cutter or gear billet be time-varying sharply. It is found that a machine with an additional motion of shaper cutter has a lower vibration, which makes it much easier to control. The reason is that the rotational inertia of shaper cutter is often much smaller than that of gear billet. Consequently, the model Eq. (26) is more valuable in application of engineering.

As shown in Fig. 4, the difference in cutting marks between the 1st (or 32nd tooth and the 16th (or 48th) one is the greatest if other schemes are adopted. The 1st tooth-flank and the 16th one on the two gears shown in Fig. 8 are imaged by SEM (5.0 kV 8.0 mm×50) [22] respectively. Imaging results of right-hand oval gear shaped by the models Eq. (26) are shown in Figs. 9(a) and 9(b). Spacing of cutting marks on the two profiles is shown in Table 1. The average spacing of each cutting mark on the profile in Fig. 9(a) is about 0.40 mm; and that in Fig. 9(b) is about 0.41 mm. Imaging results of left-hand oval gear shaped by the models Eq. (27) are shown in Figs. 9(c) and (d). Spacing of cutting marks on the two profiles is also shown in Table 1. The average spacing of each cutting mark on the profile in Fig. 9(c) is about 0.40 mm; and that in Fig. 9(d) is about 0.41 mm. It is concluded that the profile precision of every tooth shaped by the two optimal shaping models is uniform, which is in accordance with the results of simulation and analysis.

Table 1. Spacing of cutting marks on profiles. (mm)

No.	Fig. 9(a)	Fig. 9(b)	Fig. 9(c)	Fig. 9(d)
1	0.38	0.39	0.41	0.42
2	0.40	0.40	0.41	0.41
3	0.41	0.41	0.40	0.41
4	0.41	0.41	0.40	0.40
5	0.42	0.42	0.40	0.39
Average	0.40	0.41	0.40	0.41

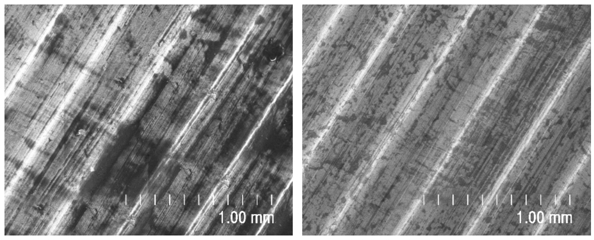

(a) The 1st tooth of right-hand one (b) The 16th tooth of right-hand one

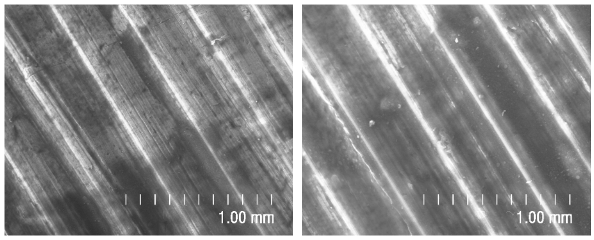

(c) The 1st tooth of left-hand one (d) The 16th tooth of left-hand one

Fig. 9. SEM (5.0 kV 8.0 mm×50) image of teeth-flank.

8. Conclusions

(1) Four methods and models of generating motion in plane have been built according to the meshing theory of non-circular gear. These methods and models include ERASCRGB, EALGB, ERAGB, and EPAGB. Virtual shaping reveals that the cutting marks among every tooth shaped by EALGB are uniform, and the accuracy among every tooth is unchanged.

Nevertheless, the accuracy among every tooth shaped by other methods is inconsistent.

(2) There are three methods of primary motion (v_z), including linkage with ω_b , linkage with ω_c , and linkage with ω_r . It can be found that the shaping force of linkage with ω_b keeps stable, and then some good dynamic performances can be obtained. However, the dynamic performances of other methods are worse.

(3) There are two methods of additional motion for helical gears, which include additional motion of shaper cutter and that of gear billet. Virtual shaping reveals that the two methods have the same precision, whether the gear has a right-hand helix or left-hand helix.

(4) According to comprehensive correlation analysis, two optimal shaping models were provided, and performed shaping experiments respectively. The experiments show that the shaping strategies and models are correct and feasible. Tooth-flank detections reveal that every tooth of the gears has the same precision using the two optimal shaping models, which is in accordance with the results of simulation and analysis. In the two optimal shaping strategies, EALGB & linkage with ω_b & additional motion of shaper cutter is easier to control, and is more valuable in application of engineering.

Acknowledgment

This work supported by Natural Science Foundation of Anhui Province (Grant No. 1408085ME94), China; and Natural Science Research Project of Higher Education of Anhui Province of China (Grant No. KJ2013A039), China.

References

[1] F. L. Litvin, I. G. Perez, A. Fuentes and K. Hayasaka, Design and investigation of gear drives with non-circular gears applied for speed variation and generation of functions, *Computer Methods in Applied Mechanics and Engineering*, 197 (8) (2008) 3783-3802.

[2] D. Mundo, G. Gatti and D. B. Dooner, Optimized five-bar linkages with non-circular gears for exact path generation, *Mechanism and Machine Theory*, 44 (4) (2009) 751-760.

[3] G. H. Yu, Z. W. Chen, Y. Zhao, L. Sun and B. L. Ye, Study on vegetable plug seedling pick-up mechanism of planetary gear train with ellipse gears and incomplete non-circular gear, *Journal of Mechanical Engineering*, 48 (13) (2012) 32-39 (in Chinese).

[4] Z. Y. Yin, C. Y. Jiang, D. T. Qin, P. X. Qiao and G. Liu, The optimization and simulation of new type non-circular gears in CVT, *Applied Mechanics and Materials*, 86 (8) (2011) 684-687.

[5] C. Lin, Y. J. Hou, H. Gong, Q. L. Zeng and L. Nie, Flow characteristics of high-order ellipse bevel gear pump, *Journal of Drainage and Irrigation Machinery Engineering*, 29 (5) (2011) 379-385 (in Chinese).

[6] G. Li, H. Li, M. H. Fang and S. C. Niu, Non-circular gear parameters of rotary transplanting mechanism calculated by reverse method, *Transactions of the Chinese Society for Agricultural Machinery*, 42 (8) (2011) 46-49 (in Chinese).

[7] X. F. Cheng and G. F. Ding, CAD/CAM and machining simulation of non-circular gear, *Machinery Design & Manufacture*, 229 (3) (2010) 61-63 (in Chinese).

[8] Y. J. Wu, J. J. Wang and Q. K. Han, Static/dynamic contact FEA and experimental study for tooth profile modification of helical gears, *Journal of Mechanical Science and Technology*, 26 (5) (2012) 1409-1417.

[9] J. L. H. Talón, J. C. C. Ortega, C. L. Gómez, E. R. Sancho and E. F. Olmos, Manufacture of a spur tooth gear in Ti-6Al-4V alloy by electrical discharge, *Computer-Aided Design*, 42 (3) (2010) 221-230.

[10] J. Yu, T. Jung, S. Kim and S. Rhee, Laser welding of cast iron and carburized steel for differential gear, *Journal of Mechanical Science and Technology*, 25 (11) (2011) 2887-2893.

[11] F. Wei and H. Lin, Multi-objective optimization of process parameters for the helical gear precision forging by using Taguchi method, *Journal of Mechanical Science and Technology*, 25 (6) (2011) 1519-1527.

[12] Y. N. Yan, S. J. Li, R. J. Zhang, F. Lin, R.D. Wu, Q. P. Lu, Z. Xiong and X. H. Wang, Rapid prototyping and manufacturing technology: principle, representative technics, applications, and development trends, *Tsinghua Science & Technology*, 14 (6) (2009) 1-12.

[13] K. D. Bouzakis, O. Friderikos and I. Tsiafis, FEM-supported simulation of chip formation and flow in gear hobbing of spur and helical gears, *CIRP Journal of Manufacturing Science and Technology*, 1 (1) (2008) 18-26.

[14] Y. Y. Liu, J. Han, L. Xia and X. Q. Tian, Hobbing strategy and performance analyses of linkage models for non-circular helical gears based on four-axis linkage, *Strojniski Vestnik-Journal of Mechanical Engineering*, 58 (12) (2012) 701-708.

[15] Y. Y. Liu, J. Han, L. Xia and G. Z. Zhang. Hobbing Process Strategy for Non-circular Helical Gears and Performance Analyses for Functional Models, *Transactions of the Chinese Society for Agricultural Machinery*, 44 (5) (2013) 281-287 (in Chinese).

[16] L. Xia, Y. Y. Liu, D. Z. Li and J. Han, A linkage model and applications of hobbing non-circular helical gears with axial shift of hob, *Mechanism and Machine Theory*, 70 (12) (2013) 32-44.

[17] F. L. Litvin and A. Fuentes, *Gear geometry and applied theory*, Second Ed. Cambridge University Press, New York, USA (2004).

[18] S. M. Blinder, *Guide to essential math*, Second Ed. Academic Press, London, UK (2013).

[19] B. W. Bair, M. H. Sung, J. S. Wang and C. F. Chen, Tooth profile generation and analysis of oval gears with circular-arc teeth, *Mechanism and Machine Theory*, 44 (6) (2009) 1306-1317.

[20] C. L. Huang, Z. H. Fong, S. D. Chen and K. R. Chang,

Profile correction of a helical gear shaping cutter using the lengthwise-reciprocating grinding method, *Mechanism and Machine Theory*, 44 (2) (2009) 401-411.

[21] J. Y. Fei, R. Deng, Z. Zhang and M. Zhou, Research on embedded CNC device based on ARM and FPGA, *Procedia Engineering*, 16 (2011) 818-824.

[22] H. SATO, M. O-Hori and K. Nakayama, Surface roughness measurement by scanning electron microscope, *CIRP Annals - Manufacturing Technology*, 31 (1) (1982) 457-462.

Youyu Liu is a researcher at Anhui Polytechnic University, and a Ph.D. Candidate at Hefei University of Technology. He received B.E. and M.E. degrees in Lanzhou University of Technology in Lanzhou, China. His research interest is manufacturing technology of non-circular gears. He has been an Associate Professor since 2012, and published more than 30 papers.